5-2019

Modeling of Electrochemical Processes at the Magnesium Anode During Struvite Formation

Tobias Dwyer

Modeling of Electrochemical Processes at the Magnesium Anode During Struvite Formation

Tobias Dwyer
University of Arkansas Department of Chemical Engineering
April 2019

Abstract

This study analyzes the current transients observed during the electrochemical formation of struvite from a solution of ammonium phosphate using a pure magnesium and magnesium alloy electrode. Through converting the chronoamperometric data to chronocoulometric data and fitting the data to various models, the driving mechanisms for struvite nucleation were elucidated. While the pure magnesium anode is controlled by only instantaneous nucleation at the electrode, the AZ31 alloy is nucleation controlled at short times and Cottrell diffusion controlled at long times.

Table of Contents

List of Figures

List of Tables

Introduction:

Fertilizer is one of the key components that has led to increased crop yields and support of a growing world population. The three key components of this fertilizer are ammonia, which is synthetically produced, potassium, and phosphate [1]. Phosphate and potassium are mined in the form of minerals, and after they are used as fertilizer are not recovered [2]. This lack of recovery can lead to eutrophication of water sources and algae growth [3]. One point of recovery could be wastewater treatment plants because runoff from crop fields and human waste contain valuable phosphate [4]. The need to recycle phosphate has led to attempts to recover the chemical through precipitation out of wastewater in the form of struvite [4]. Struvite is a salt composed of magnesium, ammonium, phosphate, and water, and as a precipitate, struvite is insoluble in water. Typical wastewater contains phosphate and ammonium ions, and so, with the addition of magnesium, struvite may be precipitated out of solution [4]. Struvite itself is a slow release fertilizer [4]. Therefore, finding a method to generate struvite from wastewater could allow for the direct generation of phosphate fertilizer.

To precipitate struvite, it is necessary to react phosphate and ammonium ions with magnesium, shown below [4].

$$Mg_{(s)} \rightarrow Mg^{2+}_{(aq)} + 2e^- \quad (1)$$

$$Mg^{2+} + NH_4^+ + PO_4^{3-} + 6H_2O \rightarrow MgNH_4PO_4 6H_2O \quad (2)$$

This addition of magnesium may be accomplished by dissolving a magnesium salt in solution [5] or through an electrochemical route where magnesium is obtained through the use of a sacrificial anode, as shown by (1). By applying a constant potential step, as is done in chronoamperometry, magnesium ions are fluxed into solution or react at the electrode surface to form struvite. While this process has shown promise for being able to recover struvite [4], there has been no attempt

to model the transients obtained at the magnesium anode from electrochemical measurements to understand the fundamental mechanisms. This is of critical importance if struvite recovery system is to be scaled up. With a working model, better estimations of struvite recovery may be made at different or varying concentrations of ammonium and phosphate. A deeper understanding of the driving mechanisms of nucleation is therefore important not just to understanding how struvite forms in this system, but to engineers seeking a physical model to predict struvite recovery from wastewater. In this study, we model the current transient obtained during the electrochemical formation of struvite to find the driving mechanism of struvite formation.

Experimental Methods:

A 0.077 M solution of Ammonium Phosphate is stirred at 260 rpm under a constant potential of -0.8 V for 6 hours. The reactor and the dimensions of the electrodes are shown in Figure 1. The anode used in the system was either pure magnesium or AZ31 alloy with a steel counter electrode. The experiment was repeated 4 times for each anode.

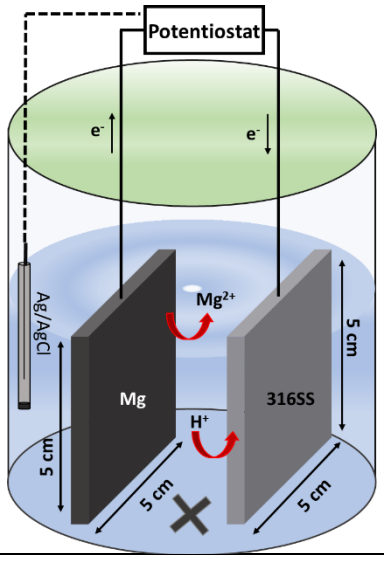

Figure 1: Schematic illustration of the electrochemical setup. A magnesium anode and steel cathode are placed under a constant potential. (Note: Figure Provided by Dr. Laszlo Kekedy Nagy)

Theoretical Methods:

There has been much work done in modeling current transients at planar electrodes. Some of the most widely used models being the Cottrell equation (diffusion controlled, planar electrode), kinetic control at a planar electrode [6], and the Scharifker-Hills [7] model of diffusion-controlled instantaneous nucleation and growth. Because of a lack of insight to what was the dominant current driving mechanism, each model was investigated for its ability to describe the current transient. Table 1 below summarizes these models for both the chronoamperometric and chronocoulometric transients.

Table 1: Summary of Current and Charge Transient Models

Model	Current Transient – I(t)	Charge Transient – Q(t)
Cottrell – Planar Diffusion Control	$I(t) = \frac{zFAD^{\frac{1}{2}}C_b}{\pi^{\frac{1}{2}}t^{\frac{1}{2}}}$	$Q(t) = \frac{2zFAD^{\frac{1}{2}}C_b t^{\frac{1}{2}}}{\pi^{\frac{1}{2}}} + Q_{dl} + nFA\Gamma_o$
Planar Kinetically Controlled	$I(t) = zFAk_f C_b e^{H^2 t} erfc\left(Ht^{\frac{1}{2}}\right)$	$Q(t) = \frac{zFAk_f C_b}{H^2}\left[e^{H^2 t} erfc\left(Ht^{\frac{1}{2}}\right) + \frac{2Ht^{1/2}}{\pi^{\frac{1}{2}}} - 1\right]$ $H = \frac{k_f}{D_o^{\frac{1}{2}}} + \frac{k_b}{D_R^{\frac{1}{2}}}$
Instantaneous Nucleation Controlled	$I(t) = \frac{zFAD^{\frac{1}{2}}c_b}{\pi^{\frac{1}{2}}t^{\frac{1}{2}}}\left(1 - \mathrm{e}^{-\left(\frac{8\pi c_b M}{\rho}\right)^{\frac{1}{2}}N_0\pi Dt}\right)$	$Q(t) = \frac{zFAD^{\frac{1}{2}}c_b}{\pi^{\frac{1}{2}}}\left\{2t^{\frac{1}{2}} - \frac{\pi^{\frac{1}{2}}\,\mathrm{erf}\left[\left(\left(\frac{8\pi c_b M}{\rho}\right)^{\frac{1}{2}}N_0\pi D\right)^{\frac{1}{2}}t^{\frac{1}{2}}\right]}{\left(\left(\frac{8\pi c_b M}{\rho}\right)^{\frac{1}{2}}N_0\pi D\right)^{\frac{1}{2}}}\right\}$

A key advantage of chronocoulometry is that a noisy current transient may be smoothed through the numerical integration process leading to plots of charge against time that are more easily interpreted. The integration of each of these models also makes clear predictions about long time current data that can be used to obtain all of the parameters for the model. In contrast,

the kinetically controlled planar and nucleation-controlled current transients must be nonlinearly fitted to the experimental data. Table 2 summarizes how each model becomes linear at long times for charge plotted against the square root of time. Note that the Cottrell equation is linear with the square root of time and a positive intercept while the other two models are linear at long times with negative y-intercepts. This allows for an initial selection between different models when modeling the chronocoulometric transient.

Table 2: Long Time Behavior of Current and Charge Transients

Model	Current Transient – I(t)	Charge Transient – Q(t)	At Long Times
Cottrell – Planar Diffusion Control	$I(t) = \frac{zFAD^{\frac{1}{2}}C_b}{\pi^{\frac{1}{2}}t^{\frac{1}{2}}}$	$Q(t) = \frac{2zFAD^{\frac{1}{2}}C_b t^{\frac{1}{2}}}{\pi^{\frac{1}{2}}} + Q_{dl} + nFA\Gamma_o$	Linear at all times
Planar Kinetically Controlled	$I(t) = zFAk_f C_b e^{H^2 t} erfc\left(Ht^{\frac{1}{2}}\right)$	$Q(t) = \frac{zFAk_f C_b}{H^2}\left[\frac{2Ht^{1/2}}{\pi^{\frac{1}{2}}} - 1\right]$	$e^{H^2 t} erfc\left(Ht^{\frac{1}{2}}\right)$ Is Negligible
Instant Nucleation Controlled	$I(t) = \frac{zFAD^{\frac{1}{2}}c_b}{\pi^{\frac{1}{2}}t^{\frac{1}{2}}}\left(1 - \mathrm{e}^{-\left(\frac{8\pi c_b M}{\rho}\right)^{\frac{1}{2}} N_0 \pi D t}\right)$	$Q(t) = \frac{zFAD^{\frac{1}{2}}c_b}{\pi^{\frac{1}{2}}}\left\{2t^{\frac{1}{2}} - \frac{\pi^{\frac{1}{2}}}{\left(\left(\frac{8\pi c_b M}{\rho}\right)^{\frac{1}{2}} N_0 \pi D\right)^{\frac{1}{2}}}\right\}$	$\mathrm{erf}\left[t^{\frac{1}{2}}\right]$ Goes to 1

For example, if the long-time chronocoulometric data is linear with a negative y-intercept, it is appropriate to fit the long-time behavior to either the nucleation model or the kinetically controlled model, obtain the appropriate parameters for the model from the linear fitting, and use those parameters in the overall model to observe whether it makes the right correction at early times. This gives a clear way to test the predictions of each model in relation to the experimental data and elucidate the current driving mechanism of the system.

Results and Discussion:

The two averaged transients obtained from data sets taken on the pure magnesium anode and the AZ31 alloy anode, shown in Figure 2, are quite different. While both curves show an initial sharp increase in current and then decay, the pure magnesium anode exhibits a much broader initial peak and eventual decay while the AZ31 transient exhibits a sharper, thinner peak and decay.

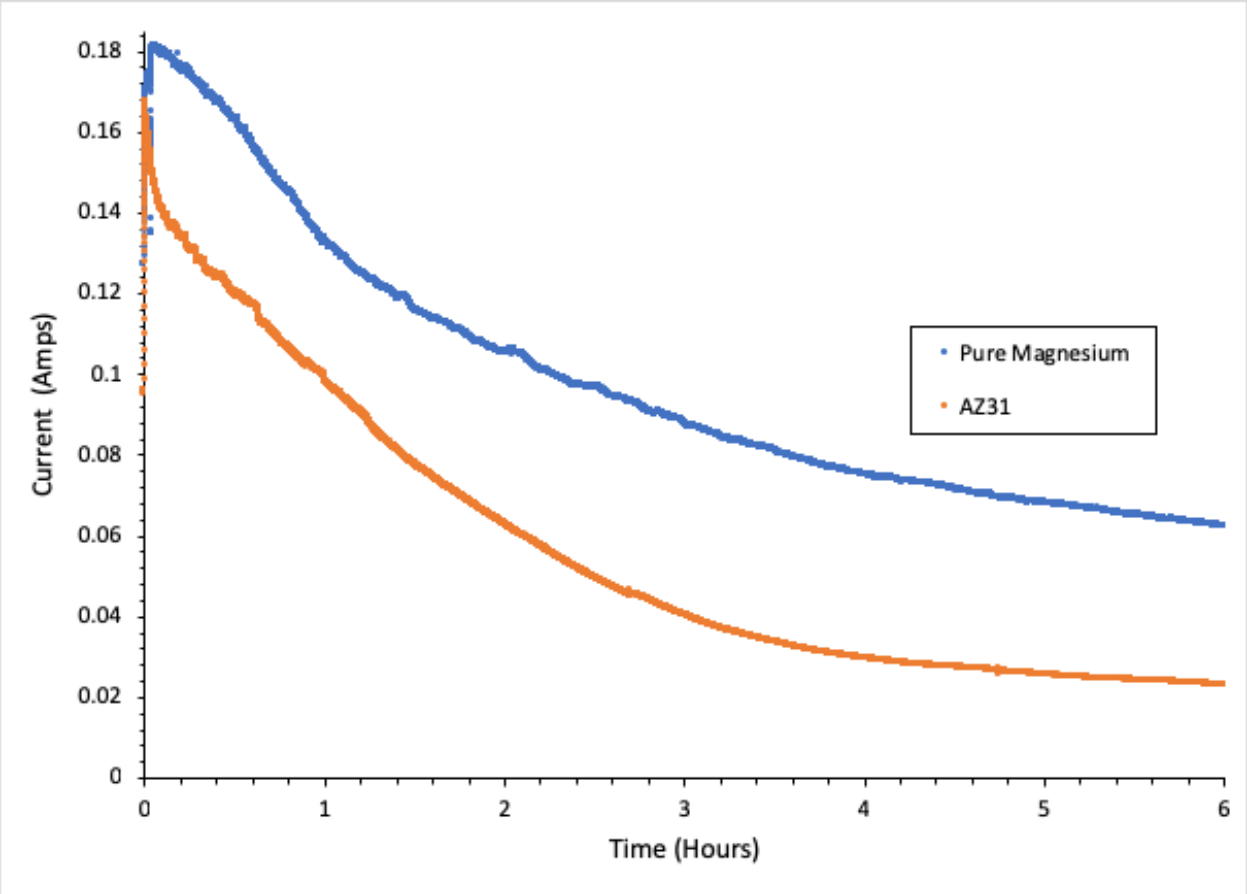

Figure 2: Average Experimental Transients for Magnesium and AZ31B alloy

To investigate the various effects that could be taking place at the anode to influence how the current decays, we constructed an Anson plot of our transient data by integrating the current data and then plotting against the square root of the time, shown in Figure 3. This treatment of

the data sheds light on possible charge transfer mechanisms. Both transients exhibit linear regions at longer times (orange and green lines for pure magnesium and AZ31 alloy, respectively). However, early time data does not exhibit a linear trend. For both anode types, at longer times, the slope of the data is linear with a negative intercept. The pure magnesium data appears to follow this trend for the entire duration of the run (orange line in Figure 3) while the magnesium alloy (AZ31) transitions into a second linear region (red line in Figure 3) with a decreased slope and positive y-intercept.

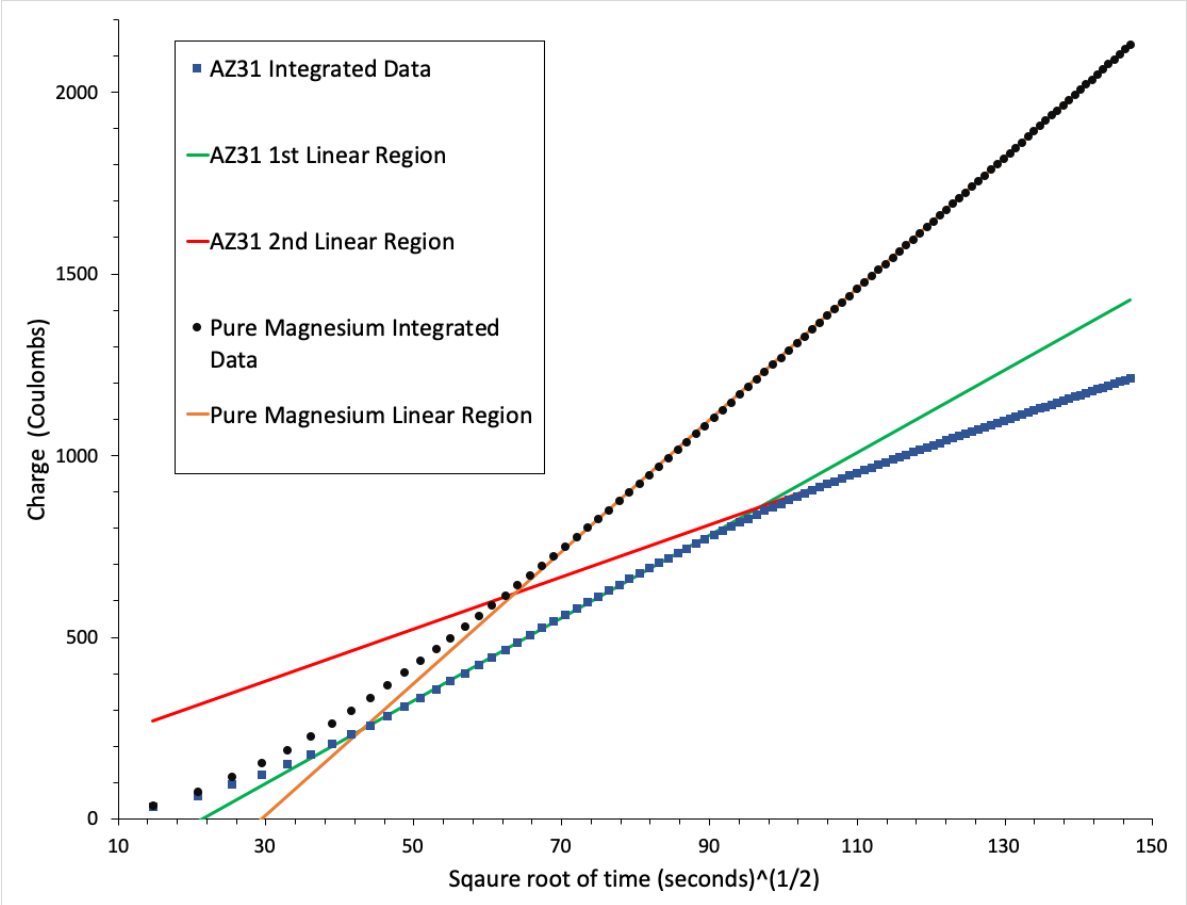

Figure 3: Anson Plots of charge vs square root of time

For the pure magnesium electrode, the two possible models shown in Table 2 are the kinetically driven and instantaneous nucleation models because they correctly describe the long-time charge behavior of the chronocoulometry data. For the kinetically driven model, the slope

and y-intercept can be used to find H, which may be substituted back into the full equation to determine if it makes the proper correction at short times. In Figure 4, we can see that the kinetic control model (green curve) significantly over shoots the experimental data, ultimately not making the proper correction. However, the instantaneous nucleation model (red curve), for which the long-time linear data is used to determine the model parameters, describes the short term chronocoulometry data well, only slightly undershooting experimental results at short times. This, therefore, gives evidence for an instantaneous, nucleation-controlled system where ammonium and phosphate ions diffuse toward the electrode and interact with the magnesium at nucleation sites and react to form struvite as an anodic deposit. 3D nucleation controlled anodic deposits have also been reported in other studies [10] but not for struvite.

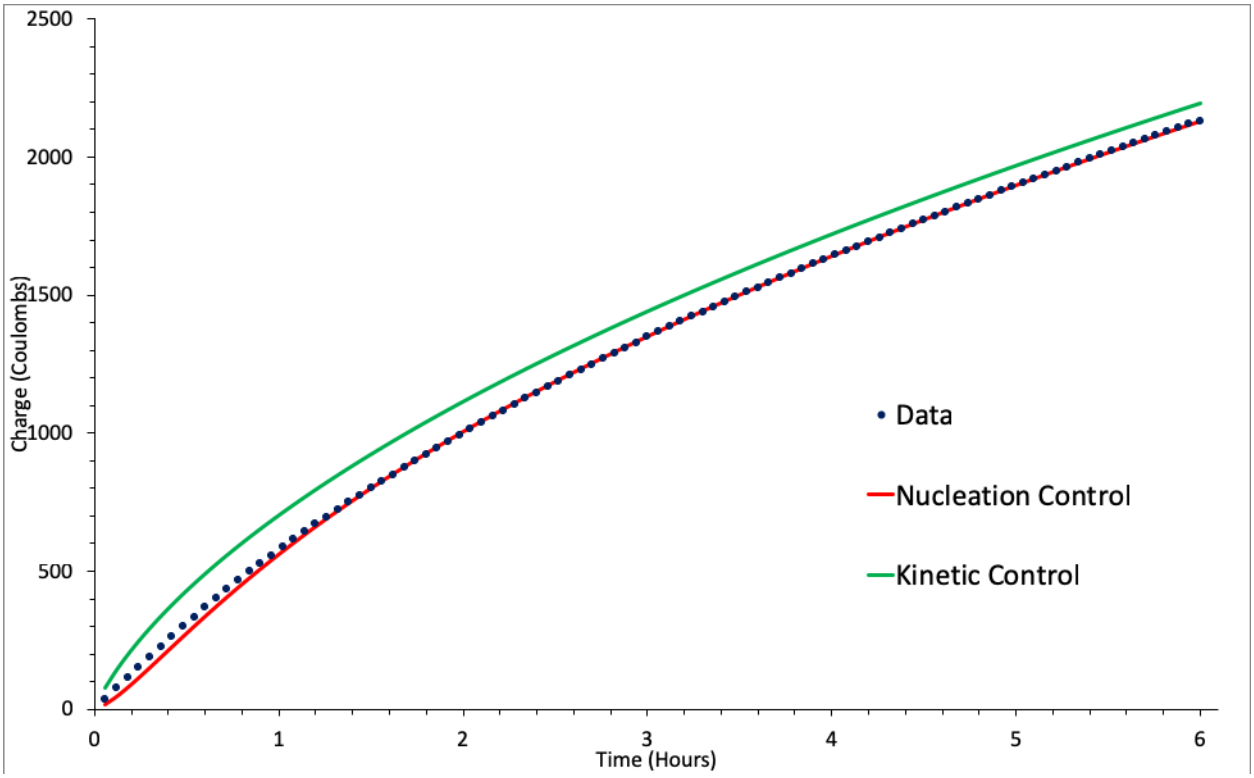

Figure 4: Time vs Charge data and model results for the pure magnesium electrode

The data for AZ31 is more nuanced. Using the first linear region to obtain instantaneous nucleation constants, we can observe the model (red curve) makes the proper correction for early chronocoulometry data in Figure 5. However, the system clearly transitions into different behavior not described by the instantaneous nucleation model. Furthermore, as was noted earlier, the behavior appears to follow a flat plate, diffusion controlled behavior exhibiting a decreased slope and positive y-intercept (orange curve).

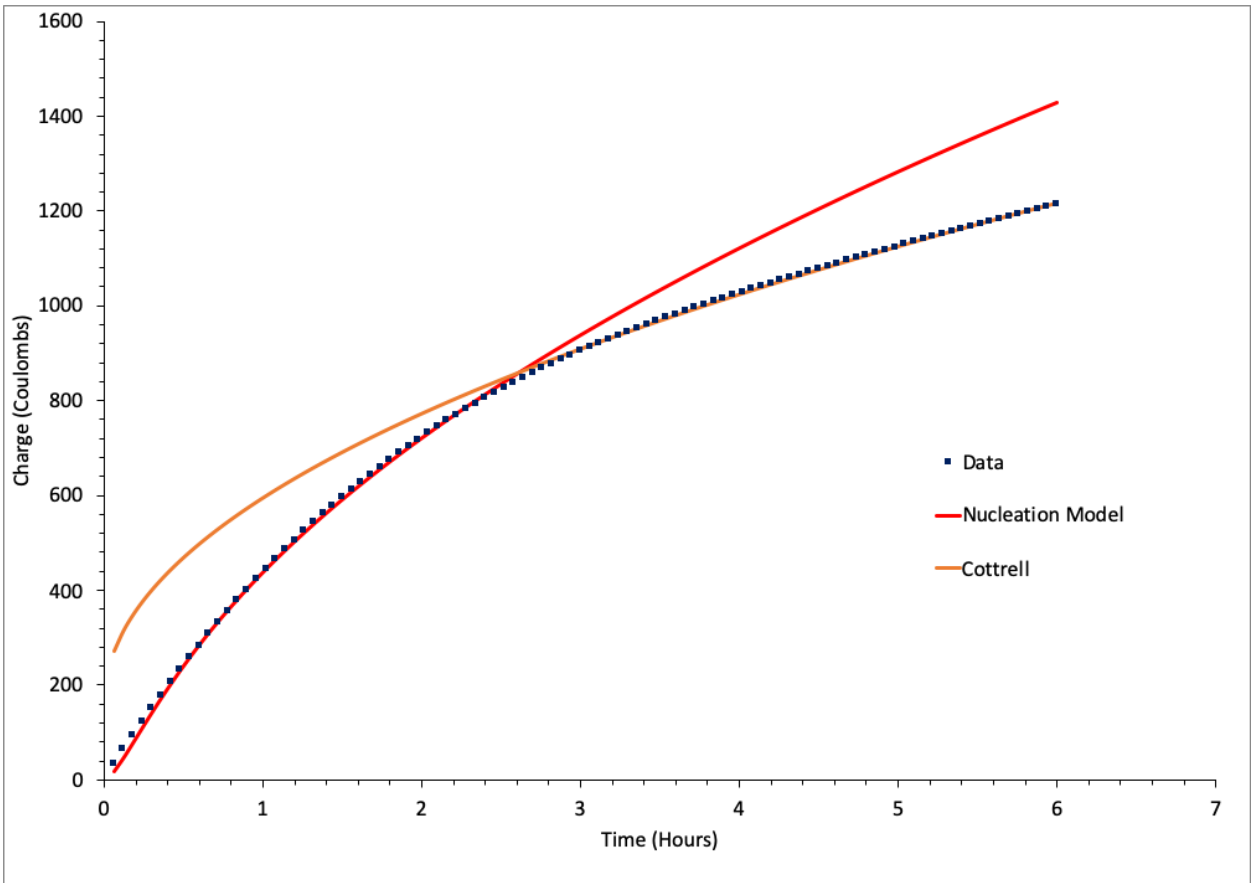

Figure 5: Time vs Charge data and model results for the AZ31 electrode

This result indicates that for the AZ31 electrode, the processes happening at the electrode are more complex than a simple instantaneous nucleation and growth model with a clear transition from nucleation and growth type behavior to a characteristic Cottrell slope and intercept. Although we were not able to find an a priori model to describe this transition, Figure 6 represents the transition from nucleation controlled to Cottrell. To represent this transition we

introduced a fitted parameter representing the fraction of the charge contribution that is 'Cottrell Controlled', θ_2 .

$$Q_{tot} = Q_{Cottrell}\theta_2 + Q_{Nucleation}(1 - \theta_2) \quad (3)$$

$$\theta_2 = 1 - \exp(-kt^m) \quad (4)$$

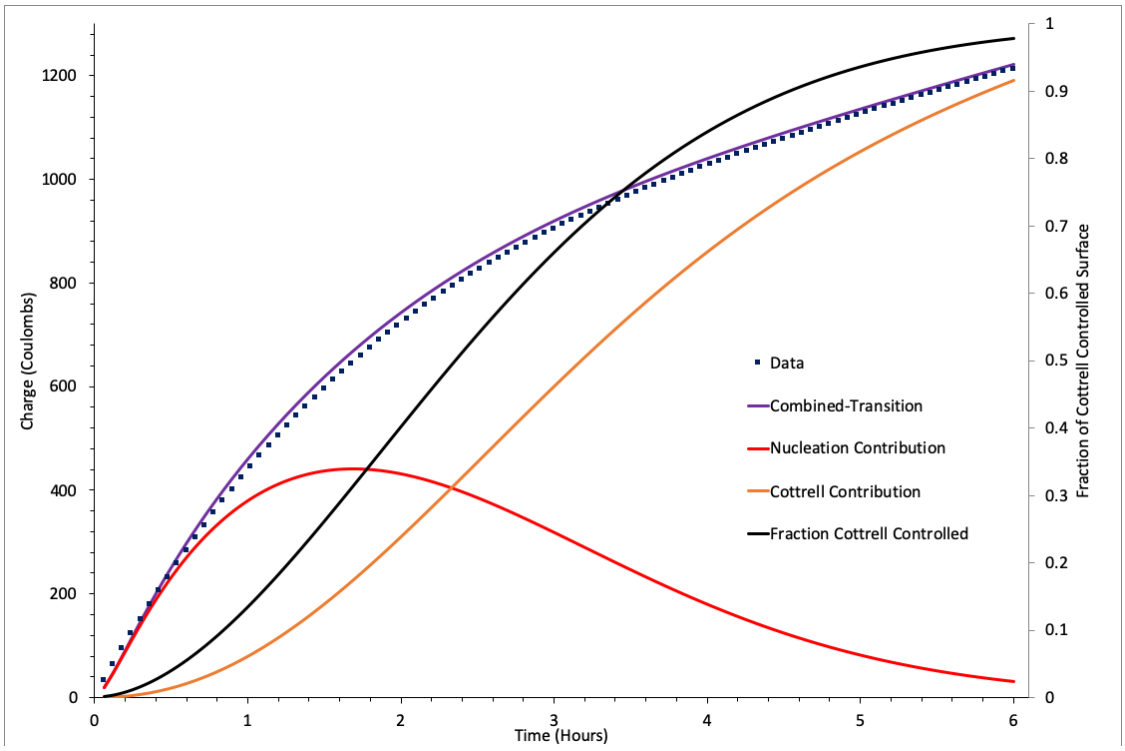

Figure 6: Empirically combined Cottrell and Nucleation Contribution

Figure 7 shows how each of the linear regions in the transient are reproduced appreciably well, as well as the transition between linear regions is also captured by this empirical relation.

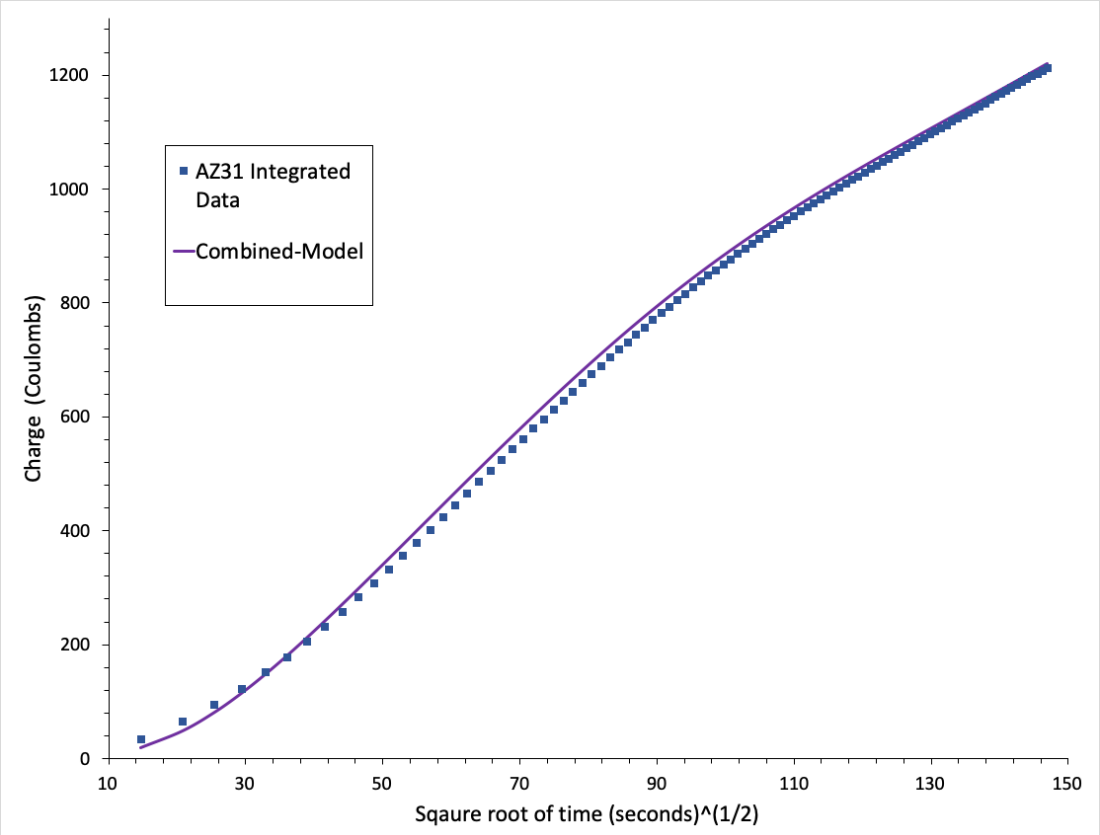

Figure 7: Reproduction of AZ31 Data

Although this change of behavior requires further investigation, some experimental observations between the difference in struvite nucleation between the two electrodes may give some clues. The struvite crystals formed on the pure magnesium electrode are porous and varied. In contrast, the AZ31 forms a compact and more uniform film of struvite at long times. This may mean at longer times, current transient is controlled not by the diffusion of ammonium and phosphate ions to the surface of the electrode as would be expected for nucleation and growth but by the diffusion of magnesium ions through the new uniform struvite film. Another interesting aspect to consider is that the alloy has areas throughout the surface that are not made of magnesium that could limit the current trasferred by formation of struvite.

Conclusions:

Nucleation and growth of struvite at a magnesium and magnesium alloy electrode were evaluated using chronocoulometry rather than the more widely used chronoamperometry. This allowed for several insights about the transients through the construction of Anson plots. It was shown that the charge transient of the pure magnesium electrode followed an instantaneous nucleation and growth model while the AZ31 alloy exhibited behavior described by different models in different regions of the transient alluding to more complex surface processes occurring at the alloy surface.

Fitting Methodology: Fitting of the experimental data to theoretical models was conducted in MATLAB using the curve fitting application for nonlinear curve fitting to 95 percent confidence bounds. The trapz function was used in numerically integrating the current data.

Acknowledgements: Thank you to Laszlo for providing the experimental data in this study and getting me involved in the project. Thank you especially to Dr. Greenlee for her support and mentorship throughout my time at the University of Arkansas. Her tireless efforts to support students including myself are impressive and truly endearing. She also provided valuable guidance and encouragement in this project. Finally, a quick thank you to Dr. Thoma for going through all of my calculations with me and helping make sure my assumptions were correct.

Works Cited

[1] Environmental Protection Agency, "Agriculture Nutrient Management and Fertilizer," 29 October 2018. [Online]. Available: https://www.epa.gov/agriculture/agriculture-nutrient-management-and-fertilizer#CommercialFertilizer. [Accessed 12 February 2019].

[2] United States Geological Survey, "Phosphate Rock Statistics and Information," 07 February 2019. [Online]. Available: https://minerals.usgs.gov/minerals/pubs/commodity/phosphate_rock/. [Accessed 13 February 2019].

[3] M. Chislock, E. Doster, R. Zitomer and A. Wilson, "Eutrophication: Causes, Consequences, and Controls in Aquatic Ecosystem," *Nature Education Knowledge,* 2013.

[4] A. Hug and K. M. Udert, "Struvite precipitation from urine with electrochemical magnesium dosage," *Water Research,* 2012.

[5] S. B. Moussa, G. Maurin, C. Gabrielli and M. B. Amor, "Electrochemical Precipitation of Struvite," *Electrochemical and Solid-State Letters,* 2006.

[6] A. Bard and L. Faulkner, "Electrochemical Methods Fundamentals and Applications Second Edition," John Wiley and Sons, Inc. , 2001, pp. 210-215.

[7] B. Scharifker and G. Hills, " THEORETICAL AND EXPERIMENTAL STUDIES OF MULTIPLE NUCLEATION," *Electrochimica Acta,* 1983.

[8] S. Xu, Y. Zhu, D. Xiong, L. Wang, P. Yang and P. K. Chu, "Zinc Electrodeposition on Polycrystalline Copper: Electrochemical Study of Early-Stage Growth Mechanism," *The Journal of Physical Chemistry C,* 2017.

[9] D. Mazaira, C. Borrás, J. Mostany and B. Scharifker, "The development of theoretical models for multiple nucleation with diffusion-controlled three- dimensional growth," in *Theoretical and Experimental Advances in Electrodeposition*, 2008.

[10] A. Hernandez-Espejel, M. Palomar-Pardave, R. Cabrera-Sierra, M. Romero-Romo, M. T. Ramires-Silvia and E. M. Arce-Estrada, "Kinetics and Mechanism of the Electrochemical Formation of Iron Oxidation Products on Steel Immersed in Sour Acid Media," *The Journal of Physical Chemistry B,* 2011.

Appendix I: Raw Experimental Data

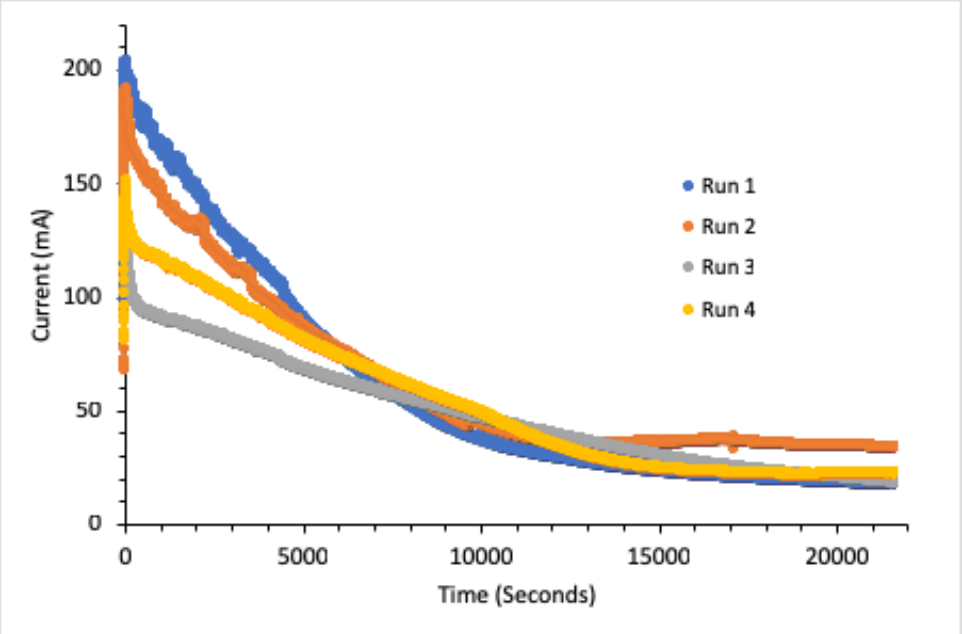

Figure 8: Raw Transients for AZ31 (Provided by Dr. Laszlo Kekedy Nagy)

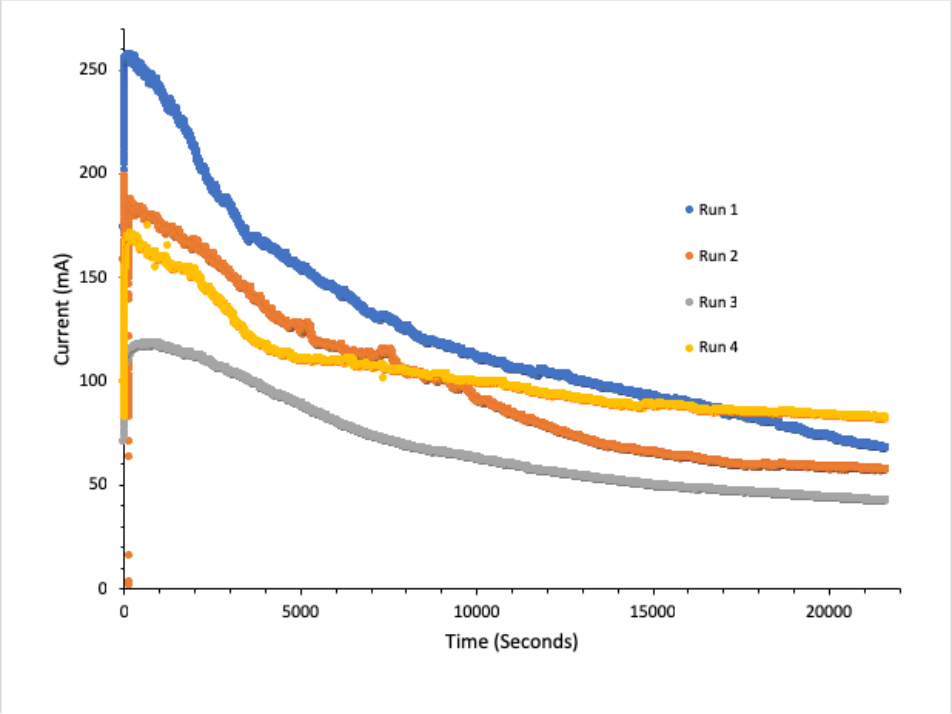

Figure 9: Raw Transients for Pure Magnesium (Provided by Dr. Laszlo Kekedy Nagy)

Appendix II: Derivation of Instantaneous Nucleation and Growth Model

This model is derived making the assumption that the continuity equation for a single hemispherical nucleus applies, that the Avrami equation can be used to account for diffusion zone overlap, and that planar diffusion fields are equivalent to the growth of the Nuclei.

Continuity equation:

$$\frac{\partial C}{\partial t} = D\left[\frac{\partial^2 C}{\partial r^2} + \frac{2}{r}\frac{\partial C}{\partial r}\right]$$

$$concentration\ is\ in\ terms\ of\ r\ and\ t$$

Initial condition

$$C(r,0) = C_b(the\ bulk\ concentration)$$

Boundary Conditions

$$C(r,t) = C_b\ as\ r \to \infty$$

$C(r_0,t) = 0$ (instant conversion at the hemisphere of radius r_0, e.g. diffusion controlled)

Take the Laplace transform of both sides

$C(r,t) = U(r,s)$ → notation for this transform

$$sU(r,s) - C(r,0) = D\left[\frac{\partial^2 U}{\partial r^2} + \frac{2}{r}\frac{\partial U}{\partial r}\right]$$

$$sU(r,s) - C_b = D\left[\frac{\partial^2 U}{\partial r^2} + \frac{2}{r}\frac{\partial U}{\partial r}\right]$$

Rearrange and solve the ODE

$$0 = D\left[\frac{\partial^2 U}{\partial r^2} + \frac{2}{r}\frac{\partial U}{\partial r}\right] - sU(r,s) + C_b$$

$$(General\ Solution)$$

$$U(r,s) = \frac{C_b}{s} + \frac{k_1 D^{\frac{1}{2}} e^{-s^{\frac{1}{2}} r/D^{\frac{1}{2}}}}{r} + \frac{k_2 D^{\frac{1}{2}} e^{s^{\frac{1}{2}} r/D^{\frac{1}{2}}}}{s^{\frac{1}{2}} r}\ (where\ k_1 and\ k_2\ are\ constants)$$

$$k_2 = 0\ because\ C(r,t) = C_b\ as\ r \to \infty\ (excluded\ on\ physical\ grounds)$$

$U(r_0,s) = 0$ because Laplace transform of 0 is 0

$$0 = \frac{C_b}{s} + \frac{k_1 e^{-s^{\frac{1}{2}} r_0/D^{\frac{1}{2}}}}{r_0} \to k_1 = -\frac{C_b r_0}{s e^{-s^{\frac{1}{2}} r_0/D^{\frac{1}{2}}}}$$

$$U(r,s) = \frac{C_b}{s} - \frac{C_b r_0 e^{-s^{\frac{1}{2}} r/D^{\frac{1}{2}}}}{s e^{-s^{\frac{1}{2}} r_0/D^{\frac{1}{2}}} r}$$

The flux at the surface of the sphere characterizes the current passed through the electrode

$$\frac{I(s)}{zFA} = D\frac{\partial U(r_0, s)}{\partial r} = D\left(\frac{C_b r_0}{s}\right)\left(\frac{1}{r_0^2} + \frac{s^{\frac{1}{2}}}{D^{\frac{1}{2}} r_0}\right) = C_b\left(\frac{D}{r_0 s} + \frac{D^{1/2}}{s^{\frac{1}{2}}}\right)$$

I(t) to get the actual expression for the current using the inverse Laplace transform

$$I(t) = zFADC_b\left(\frac{1}{r_0} + \frac{1}{D^{\frac{1}{2}}\pi^{\frac{1}{2}}t^{\frac{1}{2}}}\right)$$

The equation above is where other works have started [9], hence my derivation from first principles here. For the Scharifker-Hills model me make the assumption that the system reaches steady state quickly and so the second term in parenthesis may be considered negligible.

Therefore, the only term dictating the current transient is the diffusion-controlled growth of the hemispherical nuclei.

$$I(t) = \frac{zFADC_b}{r_0}$$

For a hemi-sphere the surface area is $2\pi r_0^2$ making the actual current

$$I(t) = 2\pi zFDC_b r_0$$

The current should also be equivalent to Faraday's law for the growth of a deposit

$$I(t) = \frac{zF\rho}{M} 2\pi r_0^2 \left(\frac{dr}{dt}\right)$$

Equate these equations, separate and integrate from 0 to t and from 0 to r_0

The radius of the growing nucleus with time is then

$$r_0 = \left(\frac{2MDC_b t}{\rho}\right)^{\frac{1}{2}}$$

We can now substitute this back into the growth for a single hemisphere

$$I(t) = 2\pi zFDC_b\left(\frac{2MDC_b t}{\rho}\right)^{\frac{1}{2}}$$

(This also happens to the current from a species coming to a surface with planar diffusion and depositing in a sphere)

Extending a single nucleus to overlapping growth of Nuclei using the Avrami theorem

This requires 2 key assumptions. 1 is that the nuclei may be reduced to 2D disks along the electrode surface and that the mass being incorporated into the 2D disks is equal to the planar diffusion of the incorporated species.

Furthermore, Avrami assumes that nucleation occurs at a number of seed sites N_0 and that the number of sites may vary with time, N_0(t).

This set the growth of the nuclei equal to the amount of analyte diffusing to them in planar diffusion zones, where r_d is the radius of the planar diffusion disk.

$$\frac{\pi z F (2DC_b)^{\frac{3}{2}} M^{\frac{1}{2}} t^{\frac{1}{2}}}{\rho^{\frac{1}{2}}} = \frac{zFC_b\left(\pi r_d^2(t)\right)}{\pi^{\frac{1}{2}} t^{\frac{1}{2}}}$$

Rearranging the equation to find $r_d(t) = (kDt)^{\frac{1}{2}}$

$$where\ k = \left(\frac{8\pi C_b M}{\rho}\right)^{\frac{1}{2}}$$

For instant nucleation without overlap surface overage fraction is

$$\theta_{ex} = N_0 \pi k D t$$

Where N_0 is the density of nuclei (Nuclei per surface area) .

The Avrami equation can then adjust for the overlap of the disks

$$\theta = 1 - \exp(-\theta_{ex})$$
$$\theta = 1 - \exp(-N_0 \pi k D t)$$

Therefore, because we assumed that the amount of analyte going to the surface equivalent to the planar diffusion going to the surface which is the planar diffusion normally at the surface times the surface covered by diffusion zones θ.

This planar diffusion can be derived from these boundary conditions.

$$\frac{\partial C}{\partial t} = D\left(\frac{\partial^2 C}{\partial x^2}\right)$$
$$C_b\ is\ the\ initial\ concentration$$
$$C(0,t) = 0$$
$$C(x,t) \text{ as } x \rightarrow \infty$$
$$i(t) = \frac{zFAC_b D^{\frac{1}{2}}}{(\pi t)^{\frac{1}{2}}}$$

Then times the available surface area not covered by nucleating diffusion zones.

$$i(t) = \frac{zFAC_b D^{\frac{1}{2}}}{(\pi t)^{\frac{1}{2}}}\theta$$

We thereby arrive back at the relating given in the theoretical section.

$$i(t) = P_1 t^{-\frac{1}{2}}(1 - \exp(-P_2 t))$$

Where $P_1 = \frac{zFAC_b D^{\frac{1}{2}}}{\pi^{\frac{1}{2}}}$

$$P_2 = N_0 D\pi \left(\frac{8M\pi C_b}{\rho}\right)^{\frac{1}{2}}$$